

A novel non-autonomous hyperchaotic map based on discrete memristor parallel connection

Weiping Wu(吴伟平), Mengjiao Wang(王梦蛟), and Qigui Yang(杨启贵)

Citation: Chin. Phys. B, 2025, 34 (**5**): 050503. DOI: 10.1088/1674-1056/adb8bc
Journal homepage: http://cpb.iphy.ac.cn; http://iopscience.iop.org/cpb

What follows is a list of articles you may be interested in

A novel approach to visual image encryption: 2D hyperchaos, variable Josephus, and 3D diffusion

Yan Hong(洪炎), Xinyan Duan(段心妍), Jingming Su(苏静明), Zhaopan Wang(王昭盼), and Shihui Fang(方士辉)
Chin. Phys. B, 2025, 34 (**4**): 040504. DOI: 10.1088/1674-1056/adacc7

Hybrid image encryption scheme based on hyperchaotic map with spherical attractors

Zhitang Han(韩智堂), Yinghong Cao(曹颖鸿), Santo Banerjee, and Jun Mou(牟俊)
Chin. Phys. B, 2025, 34 (**3**): 030503. DOI: 10.1088/1674-1056/ada7db

A color image encryption algorithm based on hyperchaotic map and DNA mutation

Xinyu Gao(高昕瑜), Bo Sun(孙博), Yinghong Cao(曹颖鸿), Santo Banerjee, and Jun Mou(牟俊)
Chin. Phys. B, 2023, 32 (**3**): 030501. DOI: 10.1088/1674-1056/ac8cdf

A novel hyperchaotic map with sine chaotification and discrete memristor

Qiankun Sun(孙乾坤), Shaobo He(贺少波), Kehui Sun(孙克辉), and Huihai Wang(王会海)
Chin. Phys. B, 2022, 31 (**12**): 120501. DOI: 10.1088/1674-1056/ac8f3a

A novel color image encryption scheme using fractional-order hyperchaotic system and DNA sequence operations

Li-Min Zhang(张立民), Ke-Hui Sun(孙克辉), Wen-Hao Liu(刘文浩), Shao-Bo He(贺少波)
Chin. Phys. B, 2017, 26 (**10**): 100504. DOI: 10.1088/1674-1056/26/10/100504

A novel non-autonomous hyperchaotic map based on discrete memristor parallel connection

Weiping Wu(吴伟平)[1,2,†], Mengjiao Wang(王梦蛟)[3], and Qigui Yang(杨启贵)[2]

[1] *Guangdong Communication Polytechnic, Guangzhou* 510000, *China*
[2] *School of Mathematical Sciences, South China University of Technology, Guangzhou* 510640, *China*
[3] *School of Automation and Electronic Information, Xiangtan University, Xiangtan* 411105, *China*

(Received 18 December 2024; revised manuscript received 8 February 2025; accepted manuscript online 21 February 2025)

Since the method of discretizing memristors was proposed, discrete memristors (DMs) have become a very important topic in recent years. However, there has been little research on non-autonomous discrete memristors (NDMs) and their applications. Therefore, in this paper, a new NDM is constructed, and a non-autonomous hyperchaotic map is proposed by connecting this non-autonomous memristor in parallel with an autonomous memristor. This map exhibits complex dynamical behaviors, including infinitely many fixed points, initial-boosted attractors, initial-boosted bifurcations, and the size of the attractors being controlled by the initial value. In addition, a simple pseudo-random number generator (PRNG) was designed using the non-autonomous hyperchaotic map, and the pseudo-random numbers (PRNs) generated by it were tested using the National Institute of Standards and Technology (NIST) SP800-22 test suite. Finally, the non-autonomous hyperchaotic map is implemented on the STM32 hardware experimental platform.

Keywords: non-autonomous discrete memristors, hyperchaotic map, initials-boosted attractors, initials-boosted bifurcations

PACS: 05.45.–a, 05.45.Pq

DOI: 10.1088/1674-1056/adb8bc **CSTR:** 32038.14.CPB.adb8bc

1. Introduction

In 1971, Chua first proposed that there exists a fourth type of circuit element in nature, the memristor, which represents the relationship between magnetic flux and electric charge and derived the mathematical model of the memristor.[1] However, limited by the processing technology at that time, the physical realization of the memristor had not been achieved. It was not until 2008 that the HP Laboratory constructed a Pt/TiO_2/Pt sandwich-layered structure device and discovered the memristive phenomenon on this device. This was also the first time to construct the physical model of the memristor.[2] The memristor can achieve 0 and 1 information storage and has the advantages of high speed, low power consumption, easy integration, simple structure, and non-volatility.[3–5] The memristor integrates the functions of storage and computing in a single device, thus becoming the core component in the non-Von Neumann computing architecture for the future integration of information storage and computing. The memristor has received extensive attention since its proposal.

In the field of chaos, the memristor has been widely introduced into various continuous chaotic systems to construct memristor-based chaotic systems. In the newly constructed memristive chaotic systems, important dynamical behaviors such as coexisting attractors,[6–9] hidden attractors,[10–14] multistability,[15–19] and hyperchaos[20–27] have been discovered. In 2020, He *et al.*[28] proposed the construction methods of DMs and discrete fractional-order memristors, providing a potential model for different applications, such as cellular neural networks, modulators, sensors, discrete chaotic systems, and programmable digital circuits. Meanwhile, the discrete chaotic system can generate hyperchaos with only two dimensions,[29] making up for the deficiency that the continuous chaotic system requires four dimensions to generate hyperchaos.[30] Therefore, DMs soon attracted widespread attention in the research of discrete chaotic systems and discrete neural networks, and a large number of research achievements on DMs have been published. Bao *et al.*[31] proposed a hyperchaotic map by paralleling two DMs using the self-feedback method. Li *et al.*[32] proposed a hyperchaotic map by coupling a memristor with a one-dimensional chaotic map. Peng *et al.*[33] proposed a DM model based on the difference theory and applied this memristor to the Henon map. Gu *et al.*[34] proposed a memristive hyperchaotic map with two memristors in cascade. Lai *et al.*[35] constructed a memristive Gaussian map by coupling a sinusoidal DM with a Gaussian map. These chaotic maps based on memristors all exhibit relatively complex dynamical behaviors. However, these are all studies on autonomous memristors, and there are few studies on non-autonomous memristors.

Inspired by Ref. [36], a discrete non-autonomous memris-

†Corresponding author. E-mail: wpwu_gdcp@qq.com

© 2025 Chinese Physical Society and IOP Publishing Ltd. All rights, including for text and data mining, AI training, and similar technologies, are reserved.

tor with non-autonomous internal perturbations was designed. Meanwhile, a non-autonomous memristive hyperchaotic map is constructed by connecting the non-autonomous memristor and the autonomous memristor in parallel. This map not only has infinitely many fixed points, but also exhibits dynamic behaviors such as initial-boosted attractors and initial-boosted bifurcations, demonstrating relatively high complexity. Compared with existing literature, the proposed non-autonomous hyperchaotic map has the capability to control the size of attractors by altering initial values. The non-autonomous discrete memristors possess excellent memory, time-varying, and nonlinear characteristics. The non-autonomous hyperchaotic map constructed based on non-autonomous memristors exhibits complex dynamical behaviors. The NIST test results indicate that map can generate PRNs with high randomness. Finally, the hardware implementation of the non-autonomous hyperchaotic map was carried out using the STM32 hardware implementation platform.

The rest of the paper is arranged as follows. In Section 2, we propose the mathematical models of the discrete non-autonomous memristor and the non-autonomous hyperchaotic map based on the non-autonomous memristor. In Section 3, we discuss the stability of the fixed points of the map and its interesting dynamical phenomena. In Section 4, we design a simple PRNG and perform NIST test on the PRN generated by it. In Section 5, we implement the non-autonomous hyperchaotic map on the STM32 hardware implementation platform. Finally, we summarize the whole paper in Section 6.

2. Mathematical models

In this section, we propose a mathematical model of new discrete non-autonomous discrete memristor and, based on this model, propose a novel non-autonomous hyperchaotic map.

2.1. Mathematical model of the discrete non-autonomous memristor

Inspired by Ref. [36], attempts were made to add non-autonomous variables to different DMs, and most of the experimental results failed to meet expectations. Interestingly, the memristor model in Ref. [37] can still maintain the characteristics of a memristor after adding non-autonomous variables. The non-autonomous memristor model with added non-autonomous variables is shown as follows:

$$\begin{cases} v_n = ((2q_n - 1)^2 + u\sin(rn)) \cdot i_n, \\ q_{n+1} = q_n + ki_n, \end{cases} \tag{1}$$

where i_n represents the input current, v_n represents the output voltage, and q_n represents the internal charge.

Set the parameters $u = 0.5$, $r = 0.05$, $k = 1$, and the discrete input current as $i_n = A\sin(wn)$. Apply discrete currents with different amplitudes A and different frequencies w to the NDM. The characteristic curves i_n–v_n are shown in Fig. 1. When fixing the parameter $w = 0.01$ and setting the parameter A to 0.1, 0.2, and 0.25 respectively, we find that the hysteresis loop increases with the increase of the amplitude A, as shown in Fig. 1(a). In addition, when fixing the parameter $A = 0.1$ and setting the parameter w to 0.01, 0.02, and 0.03 respectively, we find that the hysteresis loop shrinks with the increase of the frequency w, as shown in Fig. 1(b). This is in good accordance with the fingerprint characteristics of the memristor.

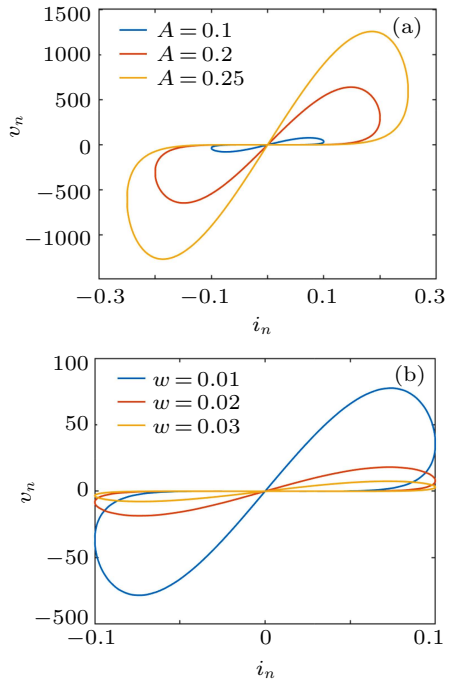


Fig. 1. The characteristic curves of the NDM model: (a) input current is $i_n = A\sin(0.01n)$ with amplitude A varying, (b) input current is $i_n = 0.1\sin(wn)$ with frequency w varying.

2.2. Mathematical model of the non-autonomous hyperchaotic map

In addition to the above NDM, we also introduce the memristor model in Ref. [38], and its mathematical model is as follows:

$$\begin{cases} v_n = \sin(\pi q_n) i_n, \\ q_{n+1} = q_n + i_n. \end{cases} \tag{2}$$

To make the constructed map model exhibit complex dynamical behaviors related to the initial values of memristors, the above two memristors are connected in parallel, and a new non-autonomous hyperchaotic map is constructed by using the self-feedback method. The structural schematic diagram of this non-autonomous hyperchaotic map model is shown in Fig. 2. After passing through two proportional controllers a and b, the discrete sequences generated by the two DMs are added together and taken as the output of the non-autonomous hyperchaotic map model, and this output is used as the input

for the next map iteration. According to the structure shown in Fig. 2, the non-autonomous hyperchaotic map model is as follows:

$$\begin{cases} x_{n+1} = a[(2y_n-1)^2 + u\sin(rn)]x_n + b\sin(\pi z_n)x_n, \\ y_{n+1} = x_n + y_n, \\ z_{n+1} = x_n + z_n, \end{cases} \tag{3}$$

where a, b, u, r, and d are control parameters. When the parameters are set as $r = 0.05$, $u = 0.02$, $a = 2.15$, $b = -1.82$, and the initial values $(x(0), y(0), z(0)) = (0.2, 0.5, 0.5)$, the map is in a hyperchaotic state, and its Lyapunov exponents (LEs) are $LE_1 = 0.2871$, $LE_2 = 0.0213$, and $LE_3 = 0$ respectively. In Fig. 3, the hyperchaotic phase diagram of the non-autonomous hyperchaotic map is shown.

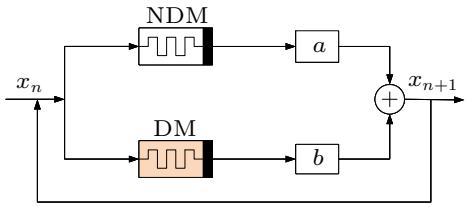


Fig. 2. Structure of the novel non-autonomous hyperchaotic map.

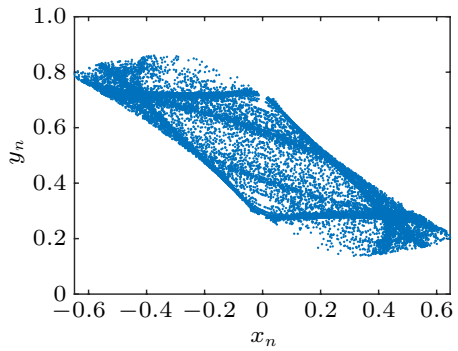


Fig. 3. Hyperchaotic phase diagram of the non-autonomous hyperchaotic map.

3. Dynamics analysis

3.1. Stability of fixed points

To analyze the stability of the fixed points of the non-autonomous hyperchaotic map, we need to obtain the fixed points of the map. The fixed points (x^*, q^*) of the map can be obtained by solving the following equation:

$$\begin{cases} x^* = a[(2y^*-1)^2 + u\sin(rn)]x^* + b\sin(\pi z^*)x^*, \\ y^* = x^* + y^*, \\ z^* = x^* + z^*. \end{cases} \tag{4}$$

We find that this map has an infinite number of fixed points, and these fixed points can be expressed as $(x^*, y^*, z^*) = (0, q^*, p^*)$, where q^* and p^* are arbitrary constants.

Furthermore, the Jacobian matrix of Eq. (3) at the fixed point $(x^*, y^*, z^*) = (0, q^*, p^*)$ is

$$J = \begin{bmatrix} a(2y^*-1)^2 + u\sin(rn) + b\sin(\pi z^*) & 0 & 0 \\ 1 & 1 & 0 \\ 1 & 0 & 1 \end{bmatrix}. \tag{5}$$

The eigenvalues of the Jacobian matrix can be easily obtained as

$$\begin{aligned} &\lambda_1 = a(2y^*-1)^2 + u\sin(rn) + b\sin(\pi z^*), \\ &\lambda_2 = 1, \quad \lambda_3 = 1. \end{aligned} \tag{6}$$

According to the stability criterion of discrete maps, at a fixed point, if the absolute value of the eigenvalue of the Jacobian matrix is less than 1, then the map is stable at this fixed point; otherwise, the map is unstable. From Eq. (6), we can see that the eigenvalues λ_2 and λ_3 are always equal to 1, but the magnitude of λ_1 is closely related to the parameters a, b, and the variable $\sin(rn)$. Therefore, the stability of the fixed points of this map is closely related to the parameters a, b, and the variable $\sin(rn)$.

Next, taking the fixed point $E_1 = (0, 1, 1)$ as an example, we discuss the influence of changes in the parameters a, b, and the variable $\sin(rn)$ on the stability of the map's fixed points. Set the parameters $u = 1$, $a = 1$, $r = 0.05$, $b = -1.82$, the relationship between the magnitude of the eigenvalue λ_1 and the variable $\sin(rn)$ is shown in Fig. 4(a). When $\sin(rn)$ is greater than 0.47, the map is in a stable state, as shown by the red region in Fig. 4(a). When $\sin(rn)$ is less than 0.47, the map is in an unstable state, as shown by the red region in Fig. 4(b). Additionally, set the parameters $u = 1$, $r = 0.05$, $a = 1$, when $a \in (-1, 4)$ the relationship between the eigenvalue and the parameter a is shown in Fig. 4(b).

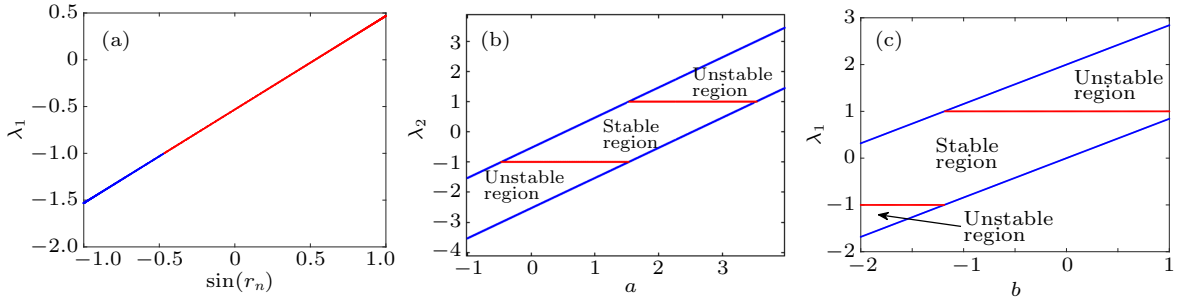


Fig. 4. Stability of the fixed point $E_1(0, 1, 1)$: (a) relationship with the variable parameter $\sin(rn)$, (b) relationship with the parameter a; (c) relationship with the parameter b.

Meanwhile, set the parameters $u = 1$, $r = 0.05$, $b = -1.82$, when $b \in (-2, 1)$, the relationship between the eigenvalue λ_1 and the parameter b is shown in Fig. 4(c). Due to the existence of the variable parameter $\sin(rn)$, when the parameters a and b take fixed values, the value of λ_1 will change within a certain region. In Figs. 4(b) and 4(c), the region between the two blue lines is the range of values of the eigenvalue λ_1 under different values of the parameter b. We use red lines to separate the stable region from the unstable region and label the different regions.

3.2. LE spectrum and bifurcation diagram

To gain a deeper understanding of the dynamical behaviors of the map, we selected different parameters to observe the LE spectrum and bifurcation phenomena of this map. Firstly, we selected parameter a as the variable parameter and set the other parameters as $r = 0.05$, $u = 0.02$, $b = -1.82$, with the initial values $(x(0), y(0), z(0)) = (0.2, 0.5, 0.5)$. The LE spectrum and bifurcation diagram of the map with respect to a are shown in Fig. 5. We can observe the dynamical behaviors of periodicity, chaos, and hyperchaos. When $a \in (-0.62, -0.57)$, the map is chaotic, and when $a \in (-0.15, 2.27)$, the map is hyperchaos.

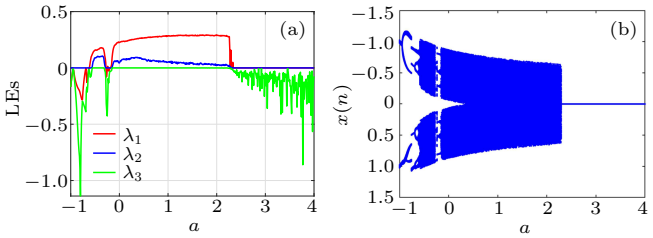


Fig. 5. When parameter $r = 0.05$, $u = 0.02$, $b = -1.82$, the bifurcation diagram and LE spectrum about the parameter a are obtained: (a) LE spectrum and (b) bifurcation diagram.

Secondly, we also chose parameter b as the variable parameter and set the other parameters as $a = 0.1$, $r = 0.05$, and $u = 0.02$. The LE spectrum and bifurcation diagram of the map with respect to b are shown in Fig. 6. Under the above parameter conditions, the dynamical behaviors of periodicity and chaos can be observed. The map exhibits hyperchaos within the parameter range of $b \in (-1.83, -1.69)$ and chaos within the parameter range of $b \in (-1.69, -1.64)$.

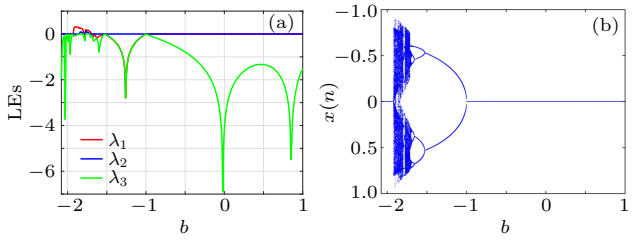


Fig. 6. When parameter $a = 0.1$, $r = 0.05$, $u = 0.02$, the bifurcation diagram and LE spectrum about the parameter b are obtained: (a) LE spectrum and (b) bifurcation diagram.

3.3. Initial-boosted attractors and initial-boosted bifurcations

In this section, we have presented the initial-boosted attractors and the initial-boosted bifurcation phenomena of the non-autonomous hyperchaotic map. This map exhibits a high degree of sensitivity to initial values. When the initial values are changed, the attractors of the map will be offseted, resulting in new attractors that have the same shape and size but are located at different positions. With the fixed parameters $a = 2.15$, $r = 0.05$, $u = 0.02$, $b = -1.82$, and by setting the initial values $(x(0), y(0), z(0)) = (0.2, 0.5, 0.5 + m\pi)$ $(m = 0, 2, 4, 6, 8)$, the attractors generated by the map under five different sets of initial values are shown in Fig. 7(a). The attractors are offseted as the initial value $z(0)$ changes. The map has different attractors for each different value of m, and these attractors are offset along the z-axis. When the value of m increases to infinity, the map can generate an infinite number of attractors.

Furthermore, under the above parameter conditions, we have found that by changing the initial value z, this map can not only produce initial-boosted attractors but also exhibit the initial-boosted bifurcation phenomenon. By setting the initial values $(x(0), y(0), z(0)) = (0.2, 0.5, 0.5 + m\pi)$ $(m = 0, 2, 4, 6, 8)$, we have demonstrated the initial-boosted bifurcation phenomena under five different sets of initial values, as shown in Fig. 7(b).

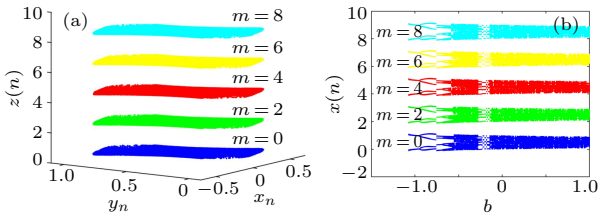


Fig. 7. Initial-boosted attractors and initial-boosted bifurcation phenomena of the map with the parameters set as $a = 2.15$, $r = 0.05$, $u = 0.02$, $b = -1.82$ and the initial values $(x(0), y(0), z(0)) = (0.2, 0.5, 0.5 + m\pi)$ $(m = 0, 2, 4, 6, 8)$. (a) Initial-boosted attractors, (b) initial-boosted bifurcation.

3.4. Control of the size of the attractor based on initial values

It was found through further experiments that this map exhibits a special kind of multistability phenomenon. The initial values of the map can not only cause offset in the attractors but also change the size of the attractors. With the parameters fixed as $a = 2.15$, $r = 0.05$, $u = 0.02$, $b = -1.82$, and the initial values set as $(x(0), y(0), z(0)) = (0.2, y_0, 0.5)$, when y_0 is within the range of $(0.31, 0.69)$, the change in y_0 can alter the size of the attractor, as shown in Fig. 8. When $y_0 \in (0.31, 0.55)$, we set the initial values of y_0 to be 0.35, 0.4, 0.45, and 0.5 respectively. It can be observed that the size of the attractor increases as y_0 increases, as depicted in Figs. 8(a)-8(d). When $y_0 \in (0.55, 0.69)$, we set the initial values of y_0 to be 0.55, 0.6, 0.65, and 0.68 respectively. It can be observed

that the size of the attractor decreases as y_0 increases, as depicted in Figs. 8(e)–8(h). Therefore, by adjusting the initial value y_0, the size of the attractors of the map can be changed to a certain extent.

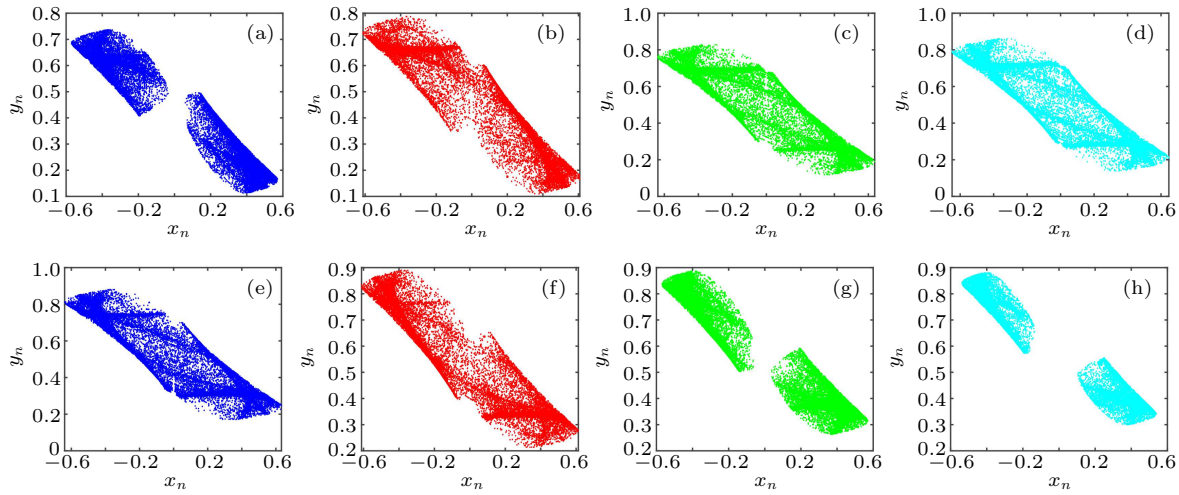


Fig. 8. Set the parameters as $a = 2.15$, $r = 0.05$, $u = 0.02$, $b = -1.82$, and the initial values $(x(0), y(0), z(0)) = (0.2, y_0, 0.5)$, the phase diagrams of the map when y_0 takes different values: (a) $y_0 = 0.35$, (b) $y_0 = 0.4$, (c) $y_0 = 0.45$, (d) $y_0 = 0.5$, (e) $y_0 = 0.55$, (f) $y_0 = 0.6$, (g) $y_0 = 0.65$, (h) $y_0 = 0.68$.

4. Pseudo-random number generator

In this section, to demonstrate the high performance of non-autonomous hyperchaotic map in PRNG, we design a simple PRNG using the non-autonomous hyperchaotic map and analyze the randomness of the generated PRNs.

4.1. Design of PRNG

A simple PRNG was designed to demonstrate the application of non-autonomous hyperchaotic maps. First, the chaotic sequence $X = \{X(1), X(2), \ldots, X(n), \ldots\}$ generated by the chaotic map is converted into a 32-bit binary stream $X_{\mathrm{B}}(n)$ for each output $X(n)$ using the IEEE 754 floating-point standard. Then, the 25th to 32nd digits in the binary stream are represented as PRN, which can be expressed as

$$P_i = X_{\mathrm{B}}(n)_{25:32}. \tag{7}$$

4.2. NIST test

To test the randomness of the PRNs generated by the proposed PRNG, SP800-22 of the NIST was applied.[39] It contains 15 sub-tests, each designed to find a non-random region of a set of binary sequences from a different perspective. Our experiment uses PRNG to generate a set of 100 binary sequences of length 10^6 and tests these binary sequences for randomness with NIST SP00-22.

The test suite contains 15 sub-tests, each of which can produce 120 P-values. First, divide the interval [0,1] into ten equal intervals. Then calculate the number of P-values for each subinterval. Finally, a χ^2 test was performed for the distribution of P-values, and P-value$_T$, was obtained. If the obtained P-value$_T$ value is greater than 0.0001, the binary sequence is considered to pass the subtest, and the test results are shown in Table 1.

Table 1. NIST SP800-22 test results for PRNs generated by a PRNG.

No.	Sub-tests	P-value$_T$	Proportion
1	frequency	0.334538	1.00
2	block frequency	0.350485	1.00
3	cumulative sums	0.851383	1.00
4	runs	0.616305	1.00
5	longest test	0.350485	0.99
6	rank	0.699313	0.99
7	FFT	0.616305	1.00
8	non-overlapping template	0.897763	1.00
9	overlapping template	0.115387	0.99
10	universal	0.719747	1.00
11	approximate entropy	0.699313	1.00
12	random excursions	0.585209	1.00
13	random excursion variant	0.484646	1.00
14	serial	0.181557	1.00
15	linear complexity	0.090936	1.00

5. Hardware implementation

Compared with continuous chaotic systems, discrete chaotic maps have better feasibility on digital experimental platforms.[40,41] In this section, we used a microcontroller card to verify the results of the numerical simulations presented in the previous sections. A microcontroller is an architecture based on a microprocessor, which includes: a microprocessor, memories (Flash, EEPROM, RAM, etc.) and I/O peripherals, all of which are combined in one box. It is programmable and sequential. The STM32F407ZGT6 microcontroller is used in this section, and its operating frequency can reach 168 MHz: this is called a digital computer with a microcontroller. It has robustness, reprogrammability, compact structure, and flexi-

bility in setting parameters and initial conditions when analyzing nonlinear dynamic systems. The STM32F407ZGT6 development board is used as part of our hardware implementation. In addition, we also used low-power 16-bit D/A converter AD5689, oscilloscopes, and other devices to form a digital experimental platform, as shown in Fig. 9.

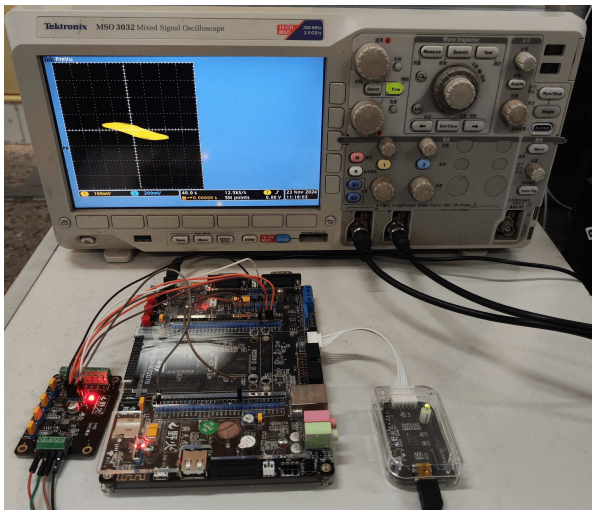


Fig. 9. Hardware implementation platform based on STM32.

The program of the discrete memristive hyperchaotic map was written in C language and downloaded onto the digital experimental platform. When the parameters $a = 2.15, r = 0.05, u = 0.02, b = -1.82$, and the initial values $(x(0), y(0), z(0)) = (0.2, y_0, 0.5)$ (y_0 is 0.35, 0.4, 0.5 respectively), the voltage and current trajectories captured by the oscilloscope are shown in Fig. 10, and their patterns are consistent with the numerical simulation results. The experimental results show that the hardware implementation of this map is feasible.

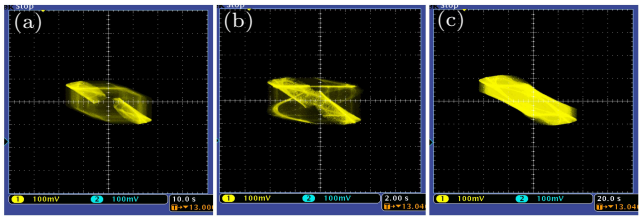


Fig. 10. Set the parameters as $a = 2.15$, $r = 0.05$, $u = 0.02$, $b = -1.82$, and the initial values as $(x(0), y(0), z(0)) = (0.2, y_0, 0.5)$. Observe the attractors of the map through an oscilloscope when y_0 takes different values: (a) $y_0 = 0.35$, (b) $y_0 = 0.4$, (c) $y_0 = 0.5$.

6. Conclusion

In this paper, a new NDM was proposed. By connecting this NDM in parallel with an autonomous DM, a novel non-autonomous hyperchaotic map was put forward. Due to the existence of the variable $\sin(rn)$ in this map, the relationship between the stability of the fixed points of the map and $\sin(rn)$ was discussed. In addition, it was discovered through experiments that by changing the initial value $z(n)$, the attractor could be offseted. Moreover, changing the initial value $y(n)$ within a certain range could adjust the size of the attractor. Therefore, we can control the size and position of the map attractor by adjusting the initial values. Finally, the hardware implementation of the map was carried out using the STM32 hardware experimental platform.

As a new type of special memristor, the NDM can be used to simulate some complex non-autonomous discrete maps in the real world such as in physics, biology, and economics. Meanwhile, it can also form non-autonomous hyperchaotic maps with different structures together with different memristors and nonlinear systems, increasing the complexity of maps at a relatively low cost and being applicable to information encryption.

Acknowledgement

Project supported by the National Natural Science Foundation of China (Grant No. 62071411).

References

[1] Chua L 1971 *IEEE Trans. Circuit Theory* **18** 507
[2] Strukov D B, Snider G S, Stewart D R and Williams R S 2008 *Nature* **453** 80
[3] Wang X, Chen X, Zhou J, Liu G, Kang S M, Nandi S K, Elliman R G and Iu H H C 2024 *IEEE Trans. Circ. Syst. I Reg. Papers* **71** 4560
[4] Wang X, Zhou J, Dong C, Jin C, Eshraghian J K, Iu H H C and Kang S M 2024 *Nonlinear Dyn.* **112** 7583
[5] Wang X Y, Zhou P F, Eshraghian J K, Lin C Y, Iu H H C, Chang T C and Kang S M 2020 *IEEE Trans. Circ. Syst. I Reg. Papers* **68** 264
[6] Ma X, Mou J, Xiong L, Banerjee S, Cao Y and Wang J 2021 *Chaos Soliton. Fract.* **152** 111363
[7] Lai Q, Wan Z, Kuate P D K and Fotsin H 2020 *Commun. Nonlinear Sci. Num. Simul.* **89** 105341
[8] Li C, Min F and Li C 1963 *Nonlinear Dyn.* **94** 2785
[9] Wang N, Zhang G and Bao H 2019 *Nonlinear Dyn.* **97** 1477
[10] Chen M, Yu J and Bao B C 2015 *Electron. Lett.* **51** 462
[11] Zhang S, Li C, Zheng J, Wang X, Zeng Z and Chen G 2021 *IEEE Trans. Circ. Syst. I Reg. Papers* **68** 4945
[12] Chen M, Li M, Yu Q, Bao B, Xu Q and Wang J 2015 *Nonlinear Dyn.* **81** 215
[13] Wang N, Cui M, Yu X, Shan Y and Xu Q 2023 *Chaos Soliton. Fract.* **177** 114242
[14] Wang X, Gao M, Iu H H C and Wang C 2022 *Chaos Soliton. Fract.* **159** 112177
[15] Guo M, Yang W, Xue Y, Gao Z, Yuan F, Dou G and Li Y 2019 *Chaos* **29** 043114
[16] Yuan F, Wang G and Wang X 2016 *Chaos* **26** 073107
[17] Yu F, Lin Y, Yao W, Cai S, Lin H and Li Y 2024 *Neural Netw.* **182** 106904
[18] Kong X, Yu F, Yao W, Cai S, Zhang J and Lin H 2024 *Neural Netw.* **171** 85
[19] Wang X, Yu J, Jin C, Iu H H C and Yu S 2019 *Nonlinear Dyn.* **96** 161
[20] Wu H G, Ye Y, Bao B C, Chen M and Xu Q 2019 *Chaos Soliton. Fract.* **121** 178
[21] Toktas F, Erkan U and Yetgin Z 2024 *Expert Syst. Appl.* **249** 123583
[22] Toktas A, Erkan U, Ustun D and Lai Q 2024 *IEEE Trans. Syst. Man, Cybern. Syst.* **54** 5237
[23] Wang M J and Gu L 2024 *Chin. Phys. B* **33** 020504
[24] Wang J, Cao Y, Mou J and Liu X 2021 *Eur. Phys. J. Special Topics* **230** 3901

[25] Erkan U, Toktas A, Memis S, Toktas F, Lai Q, Wen H and Gao S 2024 *IEEE Internet Things J.* **11** 35113
[26] Kocak O, Erkan U, Toktas A and Gao S 2024 *Expert Syst. Appl.* **237** 121452
[27] Toktas A, Erkan U, Gao S and Pak C 2024 *Appl. Math. Comput.* **462** 128340
[28] He S, Sun K, Peng Y and Wang L 2020 *AIP Adv.* **10** 015332
[29] Bao B C, Li H Z, Zhu L, Zhang X and Chen M 2020 *Chaos* **30** 033107
[30] Li Q, Hu S, Tang S and Zeng G 2014 *Int. J. Circ. Theor. Appl.* **42** 1172
[31] Bao H, Gu Y, Xu Q, Zhang X and Bao B 2022 *Chaos Soliton. Fract.* **160** 112273
[32] Li H, Hua Z, Bao H, Zhu L, Chen M and Bao B 2021 *IEEE Trans. Industr. Electron.* **68** 9931
[33] Peng Y, Sun K and He S 2020 *Chaos Soliton. Fract.* **137** 109873
[34] Gu Y, Bao, H, Xu Q, Zhang X and Bao B 2023 *IEEE Trans. Circuits Syst. II Exp. Briefs* **70** 3109
[35] Lai Q, Yang L and Liu Y 2022 *Chaos Soliton. Fract.* **165** 112781
[36] Deng Y and Li Y 2021 *Chaos Soliton. Fract.* **150** 111064
[37] Wang M, An M, Zhang X and Iu H H C 2023 *IEEE Trans. Circuits Syst. II Exp. Briefs* **70** 4251
[38] Bao H, Hua Z, Li H, Chen M and Bao B 2021 *IEEE Trans. Circ. Syst. I Reg. Papers* **68** 4534
[39] Rukhin A, Soto J, Nechvatal J, Smid M, Barker E, Leigh S, Levenson M, Vangel M, Banks D, Heckert A, James D and San V 2010 *Nat. Inst. Standards Technol., Gaithersburg, MD, USA, Special Publication* 800-22 Revision 1a
[40] Njitacke Z T, Tsafack N, Ramakrishnan B, Rajagopal K, Kengne J and Awrejcewicz J 2021 *Chaos Soliton. Fract.* **153** 111577
[41] Njitacke Z T, Koumetio B N, Ramakrishnan B, Leutcho G D, Fozin T F, Tsafack N, Rajagopal K and Kengne J 2022 *Cogn. Neurodyn.* **16** 899